Hindawi
International Journal of Optics
Volume 2019, Article ID 3618785, 18 pages
https://doi.org/10.1155/2019/3618785

Research Article

Proposal for an SDN-Like Innovative Metro-Access Optical Network Architecture

Tommaso Muciaccia[1] **and Vittorio M. N. Passaro**[2]

[1]*Telecom Italia, Rome 00163, Italy*
[2]*Department of Electrical and Information Engineering, Politecnico di Bari, Bari 70125, Italy*

Correspondence should be addressed to Tommaso Muciaccia; tommaso.muciaccia@hotmail.it

Received 5 January 2019; Accepted 19 February 2019; Published 1 April 2019

Guest Editor: Tibor Berceli

Today, telecommunication operators are facing an epochal challenge due to the need of higher reconfigurability, flexibility, and dynamicity for their networks. In the latest years, this necessity has been addressed by the introduction of Software-Defined Networking (SDN), mainly in the fields of data centers and core networks. The present work introduces a unified metro-access optical network architecture based on some features inspired by SDN models. The essential aim is to enable bandwidth shared among different passive optical networks (PONs) in order to achieve higher adaptability to increasingly migratory and volatile traffic patterns. Even if the present work is mainly focused on the architecture, several hints for specific implementation of the network nodes are detailed as well in order to demonstrate its feasibility. Several numerical simulations have been performed to assess the performance of the proposed solution both about physical effects and about quality of service. Bit error ratio degradation due to physical impairments has been evaluated and traffic congestion has been estimated in terms of burst loss probability and average throughput.

1. Introduction

The introduction of the SDN paradigm is revolutionizing the scenario of telecommunication networks, mostly for core networks and data center networks [1]. In the latest years, a few proposals inspired by the SDN model have been advanced to increase flexibility and programmability also at the edge of the network, i.e., in the metro and in the access segments.

Most of these solutions have been reviewed in a recent paper [2], even if they are not fully compliant to the Open Networking Foundation standards and definitions. Some of these proposals are focused on higher-layer reconfigurability: firstly Parol and Pawlowski in 2013 [3] and then Amokrane et al. in 2014 [4] proposed the introduction of the Open Networking Foundation SDN paradigm in the access segment, called software-defined edge network [4]; Yang et al. have proposed a software-defined access optical network architecture based on OpenFlow-enabled passive optical network in order to ensure remote unified control and service-aware flow scheduling [5]. Other recent proposals provide physical layer reconfigurability: software-defined coherent transponders which digitally process the burst transmissions according to the distance of a user from the central office have been proposed by Vacondio et al. [6]; the use of flexible grids in an access network based on OpenFlow protocol has been proposed by Cvjectic et al. [7]; intra-PON flow transmission with an optical software-defined reroute by using a quasi-passive reconfigurable node have been proposed by Yin et al. [8].

The application of the SDN approach to metro-access segment would introduce several advantages. First of all, it would allow the availability of remote management functions in the end-to-end provisioning of ultra-broadband services and the consequent optimization in the exploitation of network resources, with particular reference to the dynamic bandwidth allocation. In fact, one of the most challenging demands for the future edge networks will be the efficiency in the bandwidth usage in order to increase the network traffic adaptability for hugely variable traffic pattern (e.g., the daily variation of the traffic among the various areas in an urban

center) [9]. In fact, metro-access traffic is expected to be more strongly time-varying than backbone traffic, since the users are fewer and the averaging effect will be less impactful.

Secondly, the SDN approach would allow enhancing the performance in terms of lower congestion probability and higher quality of service (QoS). It would allow also the reduction of operational expenditures (OpEx) and total cost of ownership as well as the enabling of new business models, e.g., network as a service and bandwidth on-demand [2, 10].

In this work, an SDN-like Innovative Metro-Access Optical Network (SIMON) architecture is presented in detail. This architecture has already been presented by the authors in recent previous works [11, 12] but in this single systematic paper many more details are introduced about the possible implementation of network devices and about simulations to assess the network performances.

In order to ensure reconfigurability at the physical layer, two major SDN features have been adopted: the decoupling between the control plane and the data plane; traffic management through a centralized controller, fully aware of the entire network traffic. For this reason the network proposed has been defined SDN-like even if no reference to SDN protocol is presented.

According to the classification introduced before about recent SDN-like proposals, SIMON architecture belongs to the ones focused on physical layer reconfigurability. Compared with other proposals, the main benefits of SIMON consists in the possibility of having a full control of the network nodes allowing traffic management with a higher level of granularity without the need of optical-electrical-optical conversion for data traffic.

Moreover, the SIMON architecture merges metro and access network: the development of unified metro-access architectures is considered one of the possible evolution trends for the edge segments of telecommunication networks [10]. The simulations performed demonstrate the feasibility of a network with a reach of 50 km (without regeneration) which can be considered suitable for metro applications.

The main task performed by the central controller is traffic orchestration through the dynamic reconfiguration of the network nodes. Traffic orchestration can imply prioritization to avoid congestion and to ensure predetermined QoS.

In the following sections the network architecture is described in detail. Then the functionality of the network nodes is explained with several hints for its specific implementation. More than one technological approach is presented as possible solution to implement the most important subsystems constituting the network nodes, on the base of recent advances in optics and photonics.

2. Description of the Network Architecture

The SIMON topology is schematically represented in Figure 1. The access segment is constituted by dense wavelength-division multiplexing (DWDM) PONs, which are supposed to collect extremely heterogeneous traffic typologies, such as FTTH/FTTB access and DSLAM optical backhauling for legacy copper-based services. An increasing contribute will be due to data center interconnection and mobile backhaul and front-haul for actual LTE/4G and future 5G nodes. Especially this last traffic component will be characterized by an increasing volatility.

The adoption of DWDM in the access segment enables longer reaches thanks to the availability of higher power budget compared to conventional solutions based on time-division multiplexing (TDM), since DWDM-PONs do not require high loss power splitters [13]. Even if a great research effort is actually focused on investigating to allow the compliance of DWDM-PONs with legacy TDM-PONs by using power splitters, it can be envisioned that in the long term evolution, to which this work is addressed, DWDM-PONs will totally replace TDM-PONs, at least in several contexts. In that eventuality high loss power splitters will be replaced by low loss array waveguide gratings (AWGs) [14].

PON trees are interfaced to a metro DWDM ring through some nodes performing optical switching without optical-electro-optical conversions: this allows reduced latency and lower power consumption.

These nodes are configured by a centralized SDN-like controller topologically corresponding to the optical line terminal (OLT). The OLT is directly connected only with few network nodes, i.e., the 4-degree nodes, being the other nodes, i.e., the 3-degree nodes, indirectly connected with the OLT.

The authors have named this topology "Star-in-ring". It represents a proposal for a gradual cost-effective migration from current common ring topologies (WDM/SDH/SONET) to innovative mesh topologies, which will probably be a possible evolution for metro networks, since they are more efficient for traffic routing when compared to equivalent rings thanks to a larger availability of paths in case of link (or node) failure. A quantitative comparison between mesh and ring metropolitan optical network architectures is reported in [15, 16]. Since a full-mesh topology would be costly for a metro-access network, the proposed solution seems to be a reasonable compromise between deployment costs and performance.

With reference to Figure 1, a single fiber ring is depicted, even if also multiple fiber rings can be considered as the overlay of more than one single fiber ring: in that case, each single fiber ring serves a certain number of nodes and ONUs. The downstream signals are sent from the OLT, routed by one or more nodes, and received from the ONUs; the upstream signals are sent from the ONUs, routed by one or more nodes, and received from the OLT; the virtual private network (VPN) traffic signals are sent from an ONU, routed by one or more nodes, and received from another ONU. The OLT is the only gateway in the metro-access network to communicate with other metro-access networks. The number of DWDM channels in the metro ring is coincident with the number of ONUs in each DWDM PON tree: thanks to the introduction of nodes, each wavelength channel in the metro ring can be shared among different ONUs belonging to different trees. When no channel in the metro ring is available, congestion occurs: in order to mitigate this phenomenon, the controller assigns channels dynamically on the base of the ONU link requests and establishes a possible route path; if necessary, the

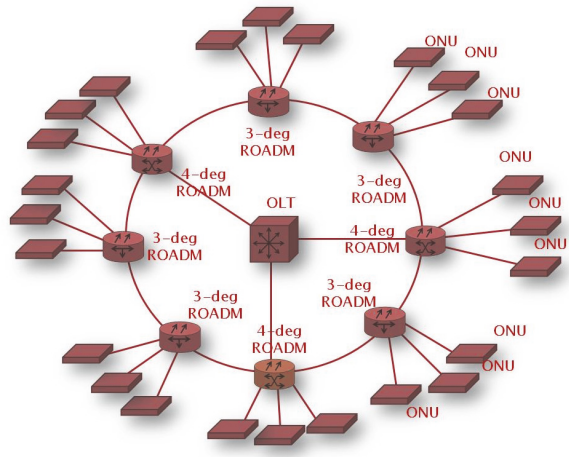

Figure 1: Star-in-ring topology of the proposed SDN-like Innovative Metro-Access Optical Network (SIMON) architecture.

controller establishes that wavelength conversion needs to be performed in the nodes (ROADMs).

In SIMON architecture, the number of ONUs (M) in each DWDM PON can be scaled up easily with few practical limitations. The proposed system is scalable up to $M = 100$ DWDM channels and more (in the figure only 3 ONUs connected to one ROADM just as an example). If M is higher, a denser packaging of wavelengths would be necessary since M is the number of channels in each DWDM link. Downstream signals are allocated in the S-band and C-band (1460 nm ÷ 1560 nm), upstream signals in the O-band (1260 nm ÷1360 nm). The bit-rate f_{BR} of each channel can be set up to 10 Gbit/s with a channel bandwidth $B_{ch} = 50$ GHz and a channel spacing $\Delta f_{ch} = 100$ GHz.

2.1. Switching Technique. Dynamic bandwidth allocation is performed through a statistical multiplexing based on optical burst switching (OBS). Burst data packets (BDPs), carrying traffic information, are preceded by burst header packets (BHPs), carrying control information for the network nodes configuration. OBS is considered one of the promising paradigms for future optical networks in synergy with OpenFlow-based SDN architecture [17]. In the SIMON architecture, OBS facilitates statistical multiplexing to efficiently share wavelength channels among multiple PON trees. OBS technique has several advantages in comparison to the other optical switching schemes. While optical channel switching allocates wavelength channels for long periods, bandwidth in OBS is reserved only for the burst duration that can theoretically vary from a single IP packet to a few milliseconds [18]. In fact, an optical burst is a number of continuous packets with the same destination. On the other hand, if compared to optical packet switching, OBS represents a more feasible solution since it can be buffer-less [18].

For the present specific architecture, a just in time signaling protocol has been adopted. In this case, BHP are sent in advance to the relative BDP and network resources are allocated immediately after the arrival of the BHP, without the necessity of an acknowledgment from the receiving node. In the proposed network, the just in time protocol is assumed as the best choice, since it is a tell-and-go protocol which does not require an acknowledgment from the BHP receiver before the BDP transmission. One-way reservation is essential because the network nodes are not able to elaborate and sending acknowledgments.

2.2. Separation of Control Plane and Data Plane. The SDN principle of separation between control and data plane is performed through polarization division multiplexing (PolDM), BHPs, and BDPs travelling over reciprocally orthogonal states of polarization (SOP). In literature, two main categories of solutions have been proposed to implement OBS, i.e., either serial header techniques, where BHPs and BDPs are separated in time domain, or parallel header techniques, where BHPs and BDPs are transmitted over different wavelengths, modulation, or coding formats [19]. PolDM enables parallel header processing. It is assumed that the network traffic signals are on-off keying (OOK) modulated in order to use simple direct detection receiver.

The spectrum of the signal transmitted by the OLT is shown in Figure 2, where both the traffic and the signaling components are represented for only one channel at $\lambda \cong 1550$ nm. A polarization combiner is used to multiplex both signals and a 50 GHz optical Gaussian filter limits their bandwidth to reduce the crosstalk among various DWDM channels.

The BHP structure is represented in Figure 3, as a comb of continuous wave (CW) discrete pulses which are set or reset for relatively long intervals of time (the burst duration). In other words, the BHP is a binary word controlling specific reconfigurable functionalities of the network nodes on the correspondent BDP channel, according to the routing strategies established by the centralized controller. The configurable elements of the nodes are the switching modules (SMs) and the tunable all-optical wavelength converters (TAOWCs). These aspects simplify the extraction of control

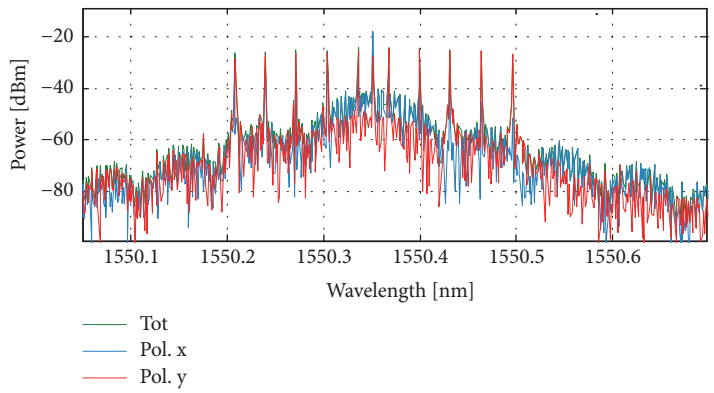

Figure 2: Transmitted signal.

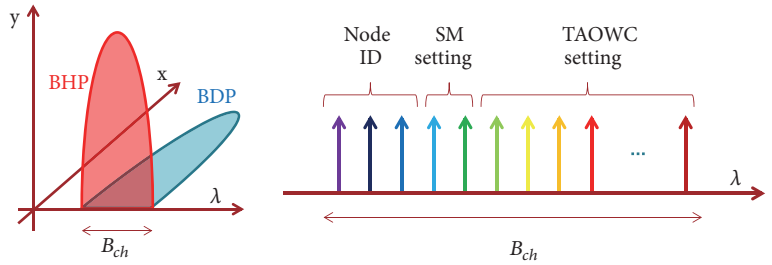

Figure 3: Burst data packets (BDP) and burst header packets (BHP) schematization.

information from the BHP, since complex techniques for timing recovery are not needed.

3. Description of the Network Nodes

Both 3-degree and 4-degree ROADMs ensure colorless, directionless, and contentionless operations [20] and have a multilayer structure, i.e., for each possible direction (north, south, east, and west); two layers are dedicated, one for upstream and one for downstream traffic. By convention, the northern direction is taken to be towards the OLT, while southern direction is referred to the DWDM PON tree corresponding to each node. 4-degree and 3-degree ROADMs are constituted by 8 layers and 6 layers, respectively. The structure of a 4-degree ROADM is shown in Figure 4(a) where, for clarity need, only the layers deputy for downstream traffic is represented. For each direction, input and output signals are combined through 1:4 modules whose simple structure is based on an optical circulator and a 1:3 coupler; a 1:4 downstream module is shown in Figure 4(b): its ports on the right are connected to the downstream layers represented in Figure 4(a). The upstream layers are connected to another analogous 1:4 upstream module in a similar way. The left ports of the two 1:4 modules, the downstream one and the upstream one, are then combined.

3.1. Structure of the ROADM Layer. The structure of a single layer is shown in Figure 5; the figure is specifically referred to a layer deputy for the traffic coming from the western direction, but the structure is analog for all the other layers.

An AWG is used for the input/output signal management for each direction, except for the southern direction which is directly connected to the DWDM PON branches. For the input direction relevant to the specific layer (the western direction for the layer shown in Figure 5), the AWG is cascaded by a wavelength converter array (WCA). The WCA can be considered a part of the layer: for this reason it is not represented in Figure 4(a). The WCA is required only in the direction for which the layer is deputy.

A further element, that is a BHP processor (BHPP), not represented in Figure 5, is interposed between the AWG and the WCA. The BHPP is constituted by an AWG, a polarization beam splitter (PBS), and a simple logic circuit. Its aim is to filter off the BHP, to extract the BHP control information, to match the ID information, and to generate the electric analog signals to drive the SMs and the TAOWCs.

The core of the layer is the switching fabric (SF) which is constituted by straight orthogonal waveguides connecting the opposite directions (north-south; east-west) and the SMs placed at their intersections.

Each SM has a simple structure, being equipped by two microring resonators (MRRs) whose resonance wavelengths are thermally tuned [21]. Since the SM has three possible output ports, two bits of each BHP are needed to configure each module.

As it is shown in Figure 6(b), the WCA is constituted by an array of tunable all-optical wavelength converters

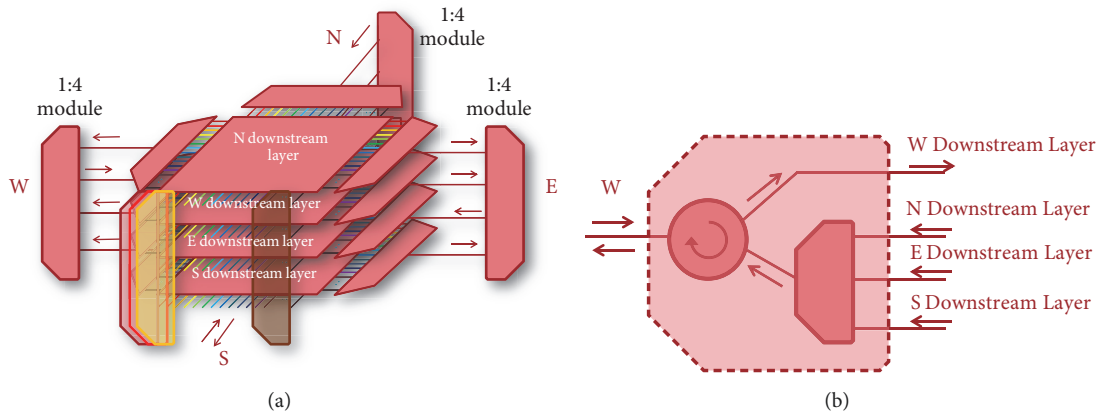

Figure 4: Multilayer reconfigurable optical add-drop multiplexer (ROADM) structure: (a) only downstream layers represented; (b) structure of a 1:4 downstream module.

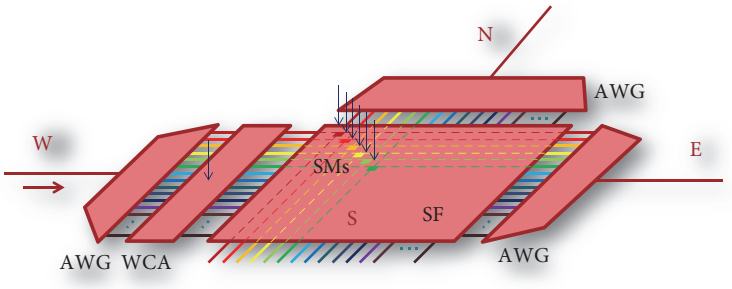

Figure 5: Structure of one of the layers constituting each reconfigurable optical add-drop multiplexer (ROADM).

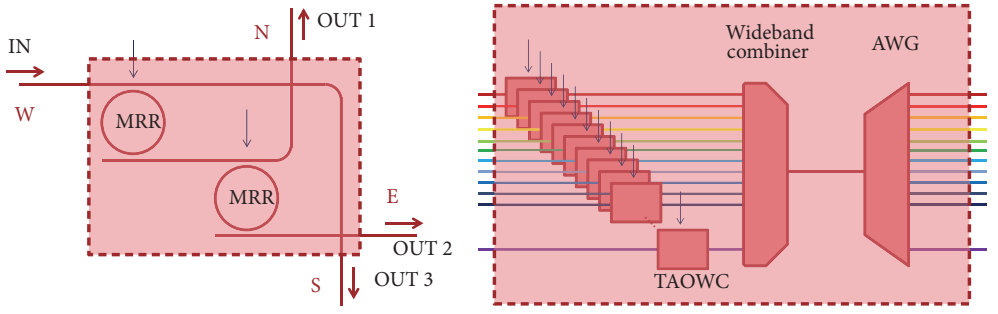

Figure 6: Structure of (a) switching module (SM); (b) wavelength converter array (WCA).

(TAOWCs), a wideband coupler and an AWG used to reorder the wavelength channels in input to the SF.

3.2. Hints for the Specific Implementation of the TAOWC. The TAOWC provides the contention-less feature to the ROADMs of the proposed SIMON architecture. Full tunability and all-optical functionality are essential requirements since they allow high flexibility and transparency for flow routing operations, respectively. In 4-degree ROADMs, the total number of TAOWC is $6M$, i.e., M converters for each direction, except to southern direction, for each layer.

3.2.1. Possible Implementation Based on SOI MRRs. A possible specific implementation of the TAOWC is schematically represented in Figure 7. It has been inspired by the work of Q. Xu et al. [22] and is based on nonlinear propagation effects in a SOI MRR: in particular, the two-photon absorption (TPA) effect, inducing the free carrier absorption (FCA), has been exploited.

The input signal, which carries the traffic information on the λ_{old} wavelength, is sent to the input port of a MRR in the add-drop configuration. The add port of the same MRR is feed by a CW signal at λ_{new} generated by a tunable

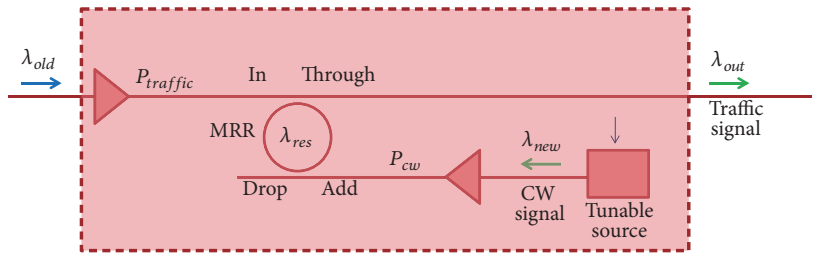

FIGURE 7: Possible implementation of the tunable all-optical wavelength converters (TAOWC) based on SOI microring resonators (MRRs).

optical source which is controlled by the information driven by the control plane. Since the possible output wavelengths are M, the source is tuned by an electrical signal which can be described by $\log_2 M$ bits.

Both the traffic and the CW signals belong to the DWDM channel grid and both of them need to be amplified in order to reach an adequate power level, that is $P_{traffic}$ and P_{cw} respectively, where $P_{traffic} \gg P_{cw}$. The output signal, available at the through port of the MRR, will carry the traffic information on the $\lambda_{out} = \lambda_{new}$ wavelength.

The behavior of the MRR in response to a high power optical input is shown in Figure 8. In few words, the optical power injected in the MRR, mainly due to the traffic input signal, determines the two-photon absorption (TPA) effect inducing the free carrier absorption (FCA). This physical effect changes the effective index n_{eff} in the waveguide of the MRR, as

$$n_{eff} = n_{eff0} + \Delta n_{eff} \quad (1)$$

where the variation $\Delta n_{eff} < 0$. As a consequence, TPA-induced FCA produces a blue shift of the transfer function of the MRR both at the through port (Figure 8(a)) and at the drop port (Figure 8(b)), implying a detuning of the resonance wavelengths $\Delta\lambda_{res}$:

$$\lambda_{res} = \lambda_{res0} + \Delta\lambda_{res} \quad (2)$$

Since the MRR transfer function is periodic, λ_{res} and λ_{res0} correspond to two series of equally spaced wavelengths. The MRR is designed in order to fulfill two basic requirements: (i) the free spectral range FSR of its transfer function corresponds to the channel spacing ($FSR = \Delta f_{ch}$); (ii) the detuning induced by the high power injection determines a blue shift $\Delta\lambda_{\text{res}}$ from λ_{res0} to λ_{res}, where the series of λ_{res} corresponds to the DWDM channel wavelengths.

Several simulations have been performed to assess the performance of the TAOWC. The MRR transfer function has been modeled on the basis of equations in literature [12, 23, 24]. The simulations of the converter have been carried out for $\lambda \cong 1550$ nm and a 1 Gbit/s OOK directly modulated signal.

Simulation results sketched in Figure 9 refer to a MRR with a large radius ($R \cong 115\ \mu$m) to achieve a $FSR = 100$ GHz. Insertion loss of the MRR is 1.05 dB at the drop port and 0.09 dB at the through port, while the filter depth is 16.7 dB at the drop port and 16.8 dB at the through port, with an estimated bandwidth of $\Delta\lambda_{3dB} = 0.074$ nm.

The change of the refractive index and the consequent blue shift of the resonance wavelength peaks are shown in Figure 9(a) as a function of the optical power $P_{traffic}$. In Figure 9(b), the extinction ratio resulting in the output converted signal is sketched, where the power of the CW tunable source is assumed to be $P_{cw} = 14$ dBm $\ll P_{traffic}$. The simulation results suggest that a $P_{traffic} \cong 23.5$ dBm is enough to induce a blue shift $\Delta\lambda_{res} \cong 0.10$ nm and an extinction ratio $ER = 24.8$ dB.

3.2.2. Possible Implementation Based on SOAs. An alternative solution to implement the TAOWC is based on semiconductor optical amplifiers (SOAs). This is a more traditional and standardized solution, since SOAs have been proposed for wavelength conversion for long time [25, 26]. Their working principle is based on nonlinear effects, such as, in most of cases, cross gain modulation: both the modulated signal at λ_{old} and the CW signal at λ_{new} are coupled into the SOA. is modulated by the gain variations depending on carrier density depleting; therefore the CW signal can carry the same information as the original input signal. SOA-based wavelength converters have been significantly improved in the latest years: error-free 320 Gbit/s wavelength conversion have been demonstrated using optical filtering technology to overcome slow recovery time of the SOA [27] and 160 Gbit/s wavelength conversion have been tested by successfully transmitting the signal over two 50 km fiber links [28]. Also tunable SOA-based wavelength converters have been proposed recently: ultrahigh-speed (320 Gbit/s) and widely tunable wavelength conversion by means of cross gain modulation using a quantum-dot SOA and a tunable CW laser [29]. Finally, low power operation have been demonstrated: typically SOA current driver circuits require few watts [30], but a wavelength converter using a SOA and a 3rd order SOI racetrack resonator integrated requiring 0.5 W has been proposed [31].

Nevertheless, if compared to the MRR-based solution previously described, SOA-based solutions appears less suitable for the specific implementation of the TAOWC since both their size (their length is typically up to one millimeter) and the materials used (typically III-V semiconductors), in most of cases, are not suitable for low-cost, highly integrated applications which are crucial in a metro/access context.

3.3. Hints for the Specific Implementation of the Optical Amplifiers. In order to compensate the losses due to the optical link (approximately 13 dB for a 50 km link) and to the 1:4 module (approximately 5 dB) and boosts the data signal in input to the TAOWC, an optical amplifier should

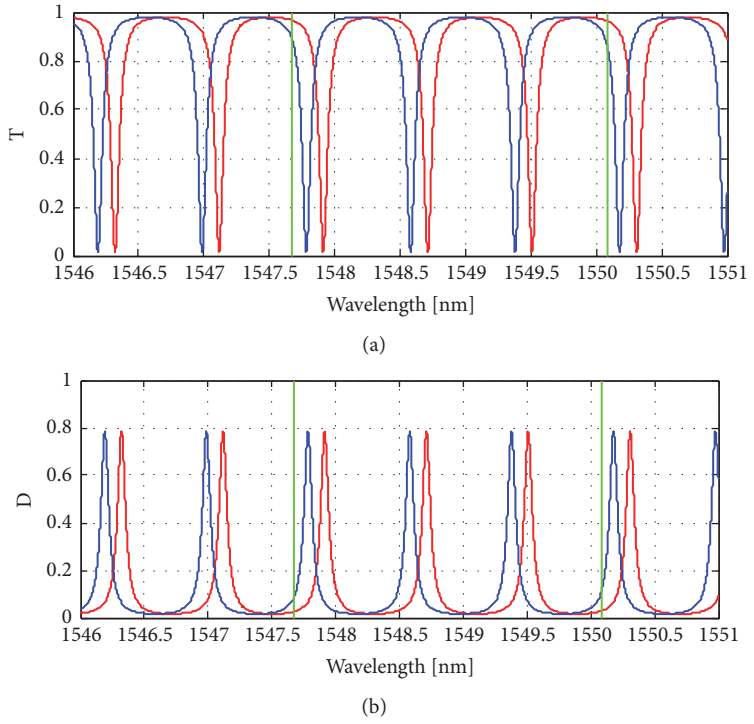

FIGURE 8: Transfer function: (a) at the through port; (b) at the drop port ($P_{traffic}$ = 24.5 dB).

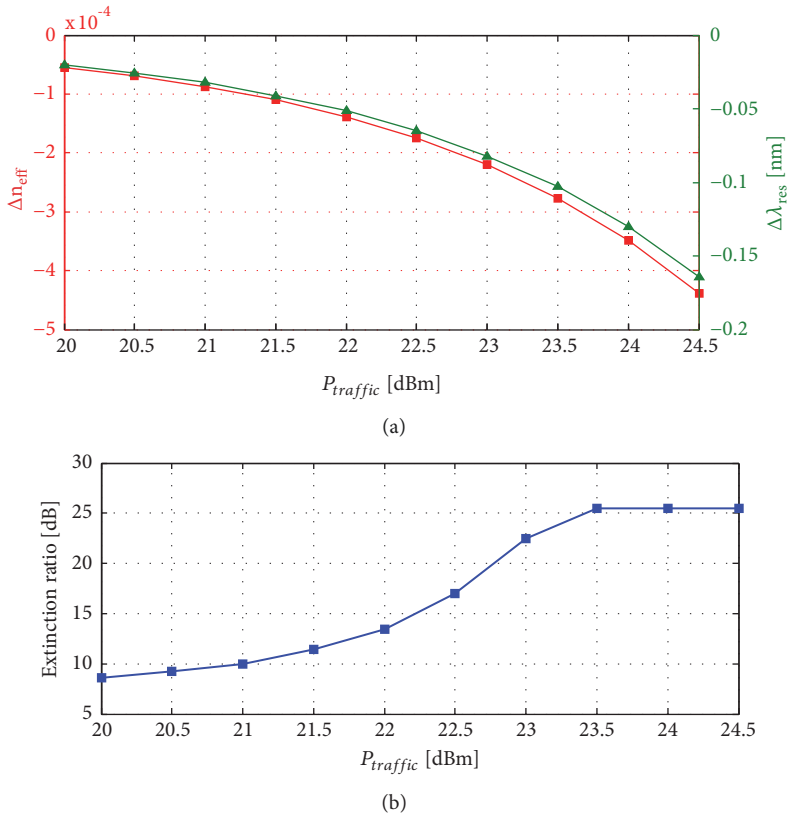

FIGURE 9: (a) Δn_{eff} (squares) and $\Delta\lambda_{res}$ (triangles); (b) extinction Ratio (ER) as a function of the traffic signal power.

be put in the input direction for each layer of the ROADM. In order to demonstrate the feasibility of the metro-access network proposed, a worst-case assumption is made: it is assumed the TAOWC implementation is based on the MRR-based described in the Section 3.2.1. In this case the estimated amplifier gain should be approximately 41.5 dB (otherwise, if SOA-base implementation would be adopted lower gain would be sufficient). In order to achieve large broadband amplification, multipump Raman amplifiers (MRAs) can be used: the use of Raman amplifiers in metro and access segment has been recently proposed [32]; the usage of MRA has recently been proposed also for PONs [33]. MRAs could be used instead of an integrated solution since the optical amplifiers can be placed outside the ROADM, before the AWG. The choice of MRAs is dictated by the necessity of large bandwidth: other more common solutions, such as Erbium-doped fiber amplifiers, would be impractical since they are characterized by narrower bandwidth. Moreover Raman amplifiers can deliver high output saturation power (23.5 dB are required in the case of MRR-based TAOWCs): since their first proposal more than 1W was guaranteed [34] and more recently also more than 10W output power has been reached [35, 36], also stimulated by sensing applications [37].

It is fair noting that the position of the optical amplifiers poses the problem of nonlinear effects which could be eventually excited in the propagation inside the AWG. This eventuality should be investigated in future works starting from already published works [38].

An alternative approach to implement the optical amplifiers is represented by SOAs; in this case the amplifiers would be integrated inside each TAOWC. In a SOA there is a trade-off between the optical gain and the output saturation power: for instance, 28.8 dB gain and 22.5 output power have been demonstrated [39]. Even higher output saturation power have been demonstrated: for instance, the maximum value of 24 dBm is demonstrated in [40] and 27.6 dBm is demonstrated in [41]. In order to achieve higher gain cascaded SOA can be considered. Among SOAs the most promising technology, which results particularly suitable to this work, is represented by quantum-dot SOAs. Theoretical simulations of quantum-dot SOAs have shown that they could achieve saturation power of 25 dBm and gain above 45 dB [42]. Quantum-dot SOAs working at 1300 nm have been demonstrated as well [43].

3.4. Power Consumption Analysis. In order to assess the feasibility of the metro-access ROADM proposed in this paper, it is useful to compare its estimated power consumption to a conventional solution. Obviously the comparison should take into account the number of users served by the node and their throughput T, i.e., the effective data rate experienced by single users when traffic congestion occurs (more rigorous definition of T will be provided in Section 6). For these reasons the following figure of merit has been considered:

$$E_{bit} = \frac{P_{node}/N_{node}}{T\,(0.5)} = \frac{\left(P_{node,intr} + P_{node,extr}\right)/N_{node}}{T\,(0.5)} \quad (3)$$

where P_{node} is the average power related to the node, N_{node} is the number of users served by the node, and $T(0.5)$ is the throughput estimated when the traffic load is 50%. The figure of merit E_{bit} is expressed in Joule and corresponds to the average energy consumed to transfer a single bit. For the present ROADM, $N_{node} = M = 100$ is considered.

The considered term of comparison is a GPON OLT, which is a very common commercially available solution. In fact, as a GPON OLT interfaces the access network with the metro segment, the present ROADM plays the same role in a converged metro-access context.

In order to carry out a fair comparison between the proposed unified metro-access network (Figure 10(a)) and a conventional metro/access network (Figure 10(b)), P_{node} includes not only the intrinsic power $P_{node,intr}$ absorbed by the node but also the extrinsic contribution $\mathrm{P_{node,extr}}$ due to the centralized metro node. The centralized metro node is represented by the centralized OLT for SIMON architecture and by an edge Ethernet switch for conventional metro/access network.

Table 1 reports the comparison of the parameters in formula (3) referred to some GPON OLTs ($P_{node,intr}$ and N_{node} reported in literature [44, 45] and in commercially available data sheet [46]) and a SIMON 4-degree ROADM.

The value considered for $T(0.5)$ in GPON OLTs is calculated as follows:

$$\mathrm{T}\,(0.5) = \frac{f_{BH}}{N_{node}/2} \quad (4)$$

where f_{BH} is the bit-rate of the OLT backhaul link towards the nearest metro node. $N_{node}/2$ is the equivalent number of active ONUs in the PON tree if traffic load is 50%.

The value considered for T(0.5) in the present ROADM is $T(0.5) = 950$ Mbit/s according to the analysis reported in Section 6 and considering a bit-rate $f_{BR} = 1$ Gbit/s.

The value considered for $P_{node,intr}$ in the present ROADM is calculated as follows:

$$P_{node} \cong 6M \bullet \left(P_{TL} + P_{TEC}\right) + 6P_{amp} \quad (5)$$

where the factor $6M$ takes into account the fact that there are 6 M TAOWC in each ROADM. $P_{TL} = \eta_{wp}P_{cw}$ is the average power consumption of the tunable laser in each TAOWC; considering a wall-plug electrical-to-optical efficiency $\eta_{wp} \cong 50\%$ and $P_{cw} = 14$ dBm, $P_{TL} \cong 50$ mW.

$\mathrm{P_{TEC}}$ is the power consumption of the thermo-electric cooler which should be necessary to ensure thermal stability of lasers. The power consumption of a thermo-electric cooler when the weighted average temperature is 40°C is $P_{TEC} = 40$ mW [47].

$\mathrm{P_{amp}}$ is the power consumption of the optical amplifier which should be considered in the input direction for each layer. Therefore there are 6 amplifiers in each ROADM. In [33] a MRA with three pumps' configuration has been proposed with a total electrical power of 405 mW for about a 25 dB optical gain over a 90 nm bandwidth. Extending this result, a value of $P_{amp} \cong 0.8$ W can be estimated to get the required gain.

The power absorption due to the BHPP can be neglected. Therefore the total power consumption of the present ROADM can be approximately considered $P_{node,intr} \cong 59$ W.

Table 1: Compared power consumption analysis.

Parameter	GPON OLT #1 [44, 45]	GPON OLT #2 [45]	GPON OLT #3 [45, 46]	Present ROADM
$P_{node,intr}$ (W)	100	1340	60	59
$P_{node,extr}$ (W)	17.8	71.3	11.1	250
P_{node} (W)	117.8	1411.3	71.1	309
N_{node}	256	1024	64	100
$T(0.5)$ (Mbit/s)	31.25	31.25	77.75	950
E_{bit} (J)	$1.47 \bullet 10^{-8}$	$4.41 \bullet 10^{-8}$	$1.43 \bullet 10^{-8}$	$3.25 \bullet 10^{-9}$

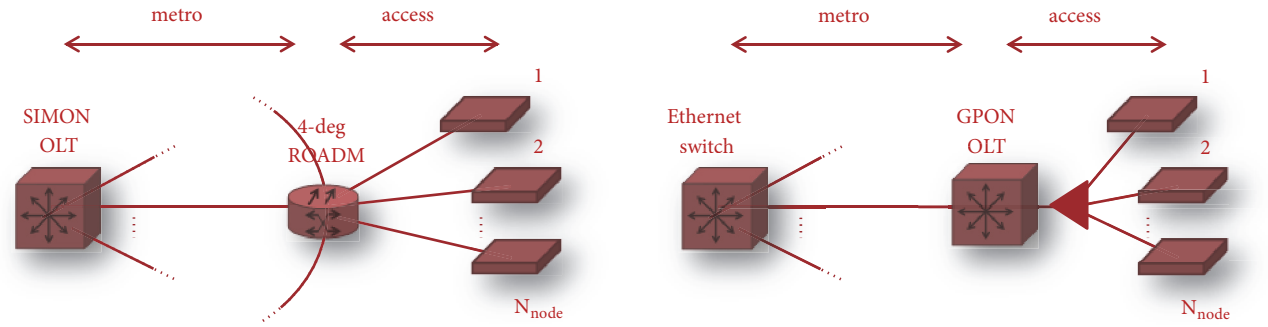

Figure 10: Compared (a) proposed SDN-like Innovative Metro-Access Optical Network (SIMON) and (b) metro/access conventional architectures.

$P_{node,extr}$ for SIMON OLT can be estimated considering the power consumption of a commercially available DWDM laser source [48]: since in the data sheet a 16 slot module needs 320 W power supply, about 2 kW can be considered for a 100 slot module. Since in the metro-access network proposed one centralized metro node corresponds to 8 access nodes (i.e., 8 ROADMs), the power contribution related to one access node is $P_{node,extr} = 250$ W.

$P_{node,extr}$ for conventional metro-access network can be estimated considering the power consumption of a commercially available Ethernet switch: the Cisco switch reported in [45] needs 3.21 kW power supply for an overall 720 Gb/s switch capacity. Therefore the power contribution related to one access node (i.e., a GPON OLT) can be estimated as follows.

$$P_{node,extr} = 3.21\ kW \bullet \frac{f_{BH}}{720\ Gb/s} \tag{6}$$

The results reported in Table 1 shows that the proposed metro-access architecture allows a significant power consumption saving, since the average energy per bit is reduced by one order of magnitude. This fact implies a significant reduction of OpEx.

Moreover, in order to evaluate the whole architecture proposed in this paper, the power consumption analysis could be extended to ONUs (compared to equivalent elements for GPON), which will be objects of future works.

Finally, it is worth noting that OpEx evaluation of the proposed SIMON architecture should take into account not only power consumption but also space saving. According to the implementation adopted for the TAOWC (MRR-based or SOA-based), its size could have an impact on the size of the ROADM and on the design of the ROADM electronic control circuit (this feature is out of the scope of the paper). The ROADM proposed could result bulkier than conventional ROADM. Anyway, since the ROADM in the proposed architecture replaces an entire OLT in a conventional architecture, a space saving can be obtained.

4. Hints for the Specific Implementation of the BHP Generator

The transmitter placed at the OLT side related to each DWDM channel is constituted by a laser modulated by data traffic, an optical source responsible for the BHP generation, and a polarization combiner. The design of the BHP generator (BHPG) will be the object of future works; in this paper only some hints are given in order to evaluate the overall feasibility of the proposed architecture.

The BHPG is based on an optical frequency comb generator (OFCG) whose function is to generate a certain number of equally spaced tones which are modulated at a rate much slower than data traffic bit-rate. The number of tones (N_{tones}) can be calculated as follows:

$$N_{tones} = \lceil \log_2 N \rceil + 2 + \lceil \log_2 M \rceil \tag{7}$$

Therefore the frequency spacing Δf_{OFCG} among the tones can be calculated as follows:

$$\Delta f_{OFCG} = \frac{B_{ch}}{N_{tones} - 1} \tag{8}$$

If $N = 8$ and $M = 100$, $\Delta f_{OFCG} \cong 4.17$ GHz.

Several technological approaches are available to realize an OFCG with such a frequency spacing. The conceptually simplest solution is to implement the OFCG through a laser array directly modulated by the BHP binary word and cascaded by an AWG: this solution is impractical because it would be excessively expensive and power consuming. Moreover it would be complicated to control wavelength stability [49]. Another possibility would be represented by a broadband laser source cascaded by a resonator which could be implemented in two variants: fiber loops [50] or MRRs [51, 52]. While the first solution has the disadvantage of being bulky, the second one has the advantage of being integrated but the size of MRRs increase with Δf_{OFCG} decreasing. Therefore both the variants of the resonator seem impractical. Furthermore a particular resonator could be represented by a single integrated mode-locked laser which can be designed to emit short pulses that have a corresponding wide optical spectrum of equally spaced phase-correlated modes. A demonstration of a mode-locked laser using a silicon evanescent laser approach with over 100 modes spaced by 0.089 nm has been proposed by Kocha et al. [49].

Another technique to generate a frequency comb is exploiting strong sinusoidal phase modulation of a CW laser which creates multiple sidebands. A scheme to achieve very flat and stable combs (10 GHz 38 comb lines in a 1 dB bandwidth) using a cascade of intensity and phase modulators driven by tailored RF waveforms has been demonstrated by Wu et al. [53]. An interesting, simple variant to this solution has been proposed by Lin et al. [54]. In that work, an OFCG is implemented by using a dual-parallel Mach-Zehnder modulator and an intensity modulator arranged in the scheme shown in Figure 11: a CW laser is modulated by the dual-parallel Mach-Zehnder modulator operated in push-pull configuration (RF frequency set at $3\Delta f_{OFCG}$); the resulting 5 comb lines are led in input to the second stage intensity modulator adjusted at the point leading to an equation of amplitude of carrier and first order sidebands in order to suppress second order sidebands (RF frequency set at Δf_{OFCG}). A spectrum of 15 comb lines with equal power can be generated, which are enough for the solution presented in this paper. Therefore this scheme can be considered the best candidate to implement the OFCG on which is based the BHPG for the present SIMON architecture. In the work by Lin et al. [54] $\Delta f_{OFCG} = 25$ GHz but it can be easily scaled down to 4 GHz by reducing frequencies of RF driving sources. If compared with the other solutions previously reviewed for the specific implementation of the BHPG, this solution appears more compact, easier to integrate, simpler, and less expensive.

5. PolDM and Nonlinear Impairments

PolDM doubles the spectral efficiency but suffers three main impairments: imperfect demultiplexing, polarization dependent losses (PDL), and polarization mode dispersion (PMD). An analysis has been carried out to evaluate the performance degradation due to these three causes, all of them generating crosstalk between the signals associated with the two different SOP and therefore inducing a degradation of the bit error ratio (BER).

Imperfections in demultiplexing are related to the misalignment $\Delta\vartheta$ between SOP of the received signal and SOP of the PBS used at the receiver. This mismatch is due to random fluctuations of SOP during the propagation along the fiber. Since the behavior of the fiber is nonstationary, the misalignment is not predictable and independent from the length L of the fiber link, so adaptive techniques have to be used. One of the proposals advanced in the past to solve this issue is related to a pilot tone on one of the two polarizations whose power drives a polarization controller [55]. In our proposed SIMON architecture, since the spectrum of the two polarizations is very different, a further pilot tone is not required. In fact, the traffic signal itself, filtered through a narrowband Gaussian filter, can be used as pilot tone. The polarization controller has to control the variable $\Delta\vartheta$ in order to maximize the power resulting from the filtering, as it can be seen from Figure 12.

In Figure 13 the effects of the polarization mismatch at the receiver are given, where both PMD and PDL have been taken into account. Performance can be considered acceptable for $|\Delta\vartheta| < 7^{\circ}$.

The effect of PDL is the attenuation of each polarization component by multiplication with different constant values. In Figure 14 the effects of PDL are shown for different values of $\Delta\alpha_{PDL}$, i.e., the additional contribution to attenuation coefficient mainly due to components with waveguide structure (couplers, buses, rings, isolators, etc.). BER degradation is due to the loss of orthogonality. Performance can be considered acceptable for $\Delta\alpha_{PDL} < 0.6$ dB.

PMD is related to optical birefringence of optical fibers which is due to the nonuniform elliptical cross section of the fiber core. PMD induces different propagation velocity of the two polarization components, which produces a differential group delay between them. PMD cannot be avoided since both data and control signals are distributed on both polarization components travelling along fiber because of the unavoidable depolarization effect. The differential group delay is the result of a stochastic process but can be estimated as follows:

$$\Delta\tau = \Delta\tau_{p1} + \Delta\tau_{p1}\omega \tag{9}$$

$$\Delta\tau_{p1} \cong 3D_{p1}\sqrt{L} \tag{10}$$

$$\Delta\tau_{p2} \cong 5D_{p2}L \tag{11}$$

where $D_{p1} = 0.1$ ps/$\sqrt{\mathrm{km}}$ and $D_{p2} = {D_{p1}}^2/12$. Performance has been assessed over length ranging and the results of the simulations are sketched in Figure 15.

Even if the physical effects of a real fiber optics link have been considered, the simulations described previously are referred to a single isolated DWDM channel. In a multichannel DWDM system, fiber nonlinearities have to be taken into account, because they generate crosstalk interference causing BER degradation. In the following simulations, a number of 10 DWDM channels have been considered for both upstream and downstream directions; a channel bandwidth B_{ch} =

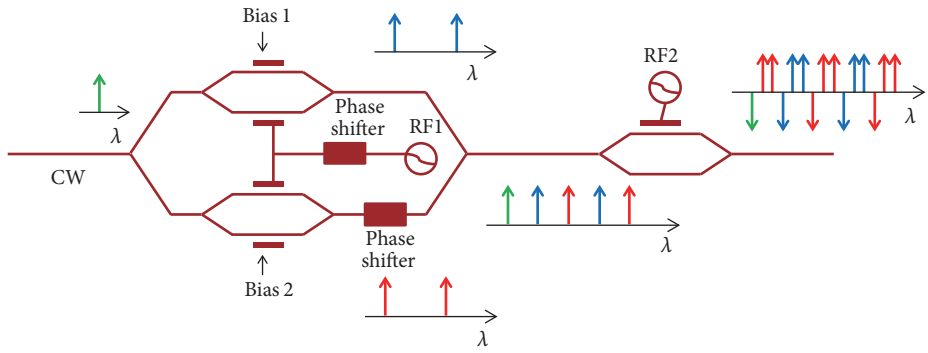

Figure 11: Scheme of the best candidate for the optical frequency comb generator (OFCG) to be implemented in the BHP generator (BHPG).

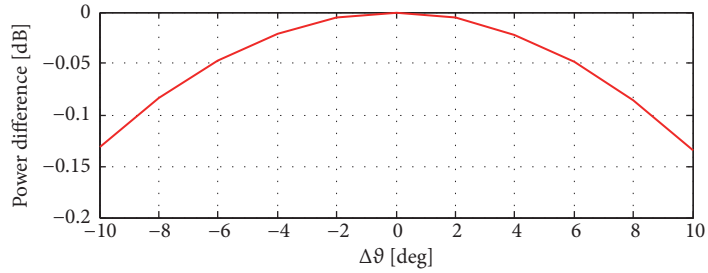

Figure 12: Pilot tone power versus $\Delta\vartheta$ ($P_{Rx} = -19.4$ dB, L = 60 km, $\Delta\alpha_{PDL} = 0.03$ dB, and $f_{BR} = 10$ Gbit/s).

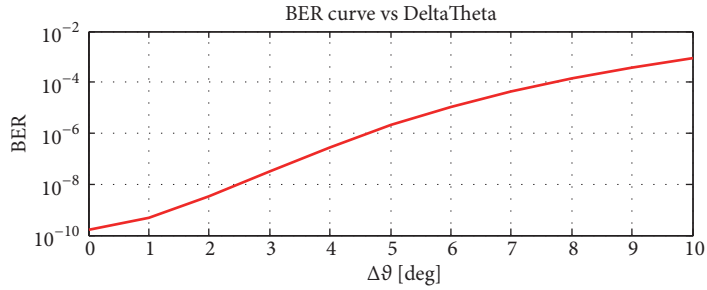

Figure 13: BER degradation due to $\Delta\vartheta$ ($P_{Rx} = -19.4$ dB, L = 60 km, $\Delta\alpha_{PDL} = 0.03$ dB, and $f_{BR} = 10$ Gbit/s).

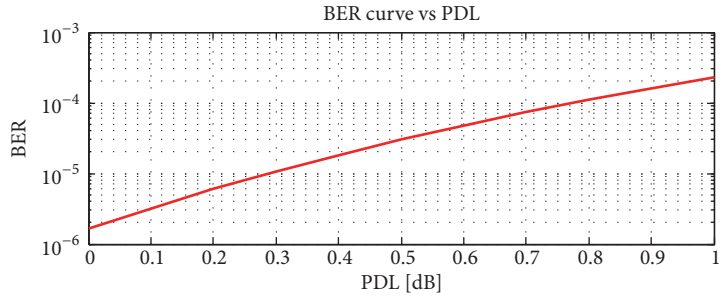

Figure 14: BER degradation due to PDL ($P_{Rx} = -19.4$ dB, L = 60 km, $\Delta\vartheta = 5^\circ$, and $f_{BR} = 10$ Gbit/s).

50 GHz and a channel spacing $\Delta f_{ch} = 100$ GHz have been adopted. Only upstream simulations have been performed in the hypothesis that traffic and data signals of each channel are copropagating.

Nonlinear effects related to refractive index have been taken into account: self-phase modulation, cross-phase modulation, and four-wave mixing. These effects have been modeled by using the following fiber parameters: effective area $A_{eff} = 80\ \mu m^2$; nonlinear refractive index $n_2 = 2.6 \bullet 10^{-20}\ m^2/W$. Also nonlinear effects related to scattering have been taken into account: stimulated Raman scattering is modeled through a fractional Raman contribution $\rho = 0.18$.

Figures 16(a) and 16(b) show BER curves versus optical launch power (P_{Tx}) considering several lengths for the optical

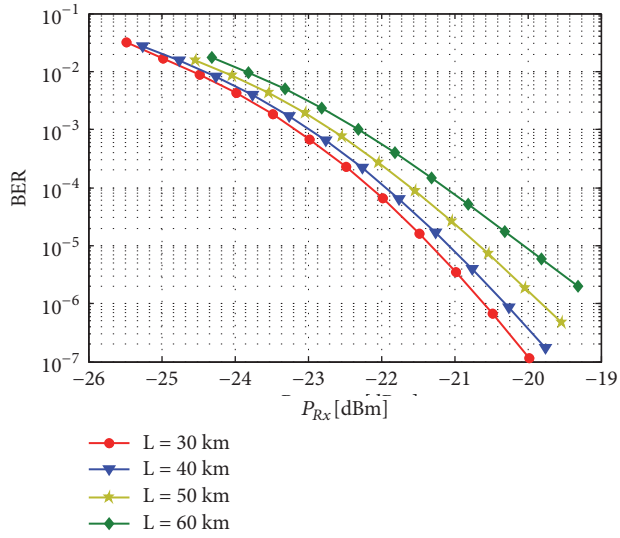

FIGURE 15: BER curves versus received power for different lengths (L = 50 km, $\Delta\alpha_{PDL}$ = 0.03 dB, $\Delta\vartheta = 5^{\circ}$, and f_{BR} = 10 Gbit/s).

link. Performances both in upstream and in downstream directions are assessed for the central channel of the DWDM channel group. BER curves denote an evident concavity: for low power values an increasing of launch power implies better performance until a critical power value is reached; after this value, the increasing of launch power implies worse performance due to the predominance of nonlinear impairments.

6. Traffic Management and Quality of Service

All the deliverable services can be referred to three basic traffic typologies: downstream (DS) traffic; upstream (US) traffic and VPN traffic (i.e., direct transmission between ONUs of the same PON or of different PON trees). For all the three traffic typologies, the BHPs are always sent by the OLT.

The DS traffic is managed as follows: BHPs are sent from the OLT to the nodes involved in the route to configure their SFs; BDP are sent from the OLT as well and automatically routed towards the receiving ONU. Collisions cannot occur since all the DS traffic is synchronously managed by the controller.

On the other hand, the US traffic is managed as follows: BHPs are sent from the OLT to configure the nodes and BDPs are sent from the transmitting ONU. In order to avoid collisions, ONUs requests have to be made synchronous.

Therefore, for the upstream traffic, a mechanism of dynamic bandwidth assignment has been adopted, inspired by the technique actually used in standard GPONs for time-division multiple access [56]. Periodical grants are sent by the OLT to the ONUs and a single time slot is allocated for each of them by default. The number of time slots assigned to each ONU can be increased or decreased on the basis of bandwidth consumed by the ONU itself.

In a VPN communication, it has been conventionally established that the client ONU uses upstream bandwidth and the server ONU uses downstream bandwidth. In a VPN context, the traffic generated from both sides is managed as US traffic, since the BHPs are sent from the OLT. The traffic generated from the "client ONU" is carried in the US bandwidth, while the traffic generated from the "server ONU" is carried in the DS bandwidth. The VPN instantiation starts with a preliminary request to the controller from the "client ONU" through an US message.

One of the greatest advantages of the proposed metro-access architecture is the possibility of managing traffic data thanks to a centralized control based on the awareness of the whole network. Traffic management can optimize the routing operations and increase the network throughput and QoS for each end-to-end communication. Overall network performances are deeply related to the software running at the application layer in the controller which can improve resources exploitation. Anyway, minimum intrinsic performances are dependent on network topology and features.

A Monte Carlo simulation has been performed to demonstrate the intrinsic network performances. Only the upstream direction has been simulated but the results obtained can be also applied in the downstream direction, since the behavior of the network is perfectly symmetrical (the network management mechanisms are the same both for upstream and for downstream traffic). The aim of this analysis is simulating the normal operation of the network in a generic instant. A certain percentage of the ONUs (rate) is active and sends a link request to the controller, i.e., they ask the controller to transmit data towards the OLT or towards other ONUs belonging to the same or to a different WDM PON. If the link request is successful, the data transmission is enabled (assumed at the full available rate f_{BR}). If the transmission to be enabled is not between ONUs of the same PON, the controller has to search a free route between different nodes of the network and, if possible, allocate resources (channels) between all the nodes involved in the route. In each iteration of the Monte Carlo analysis a certain number of link requests

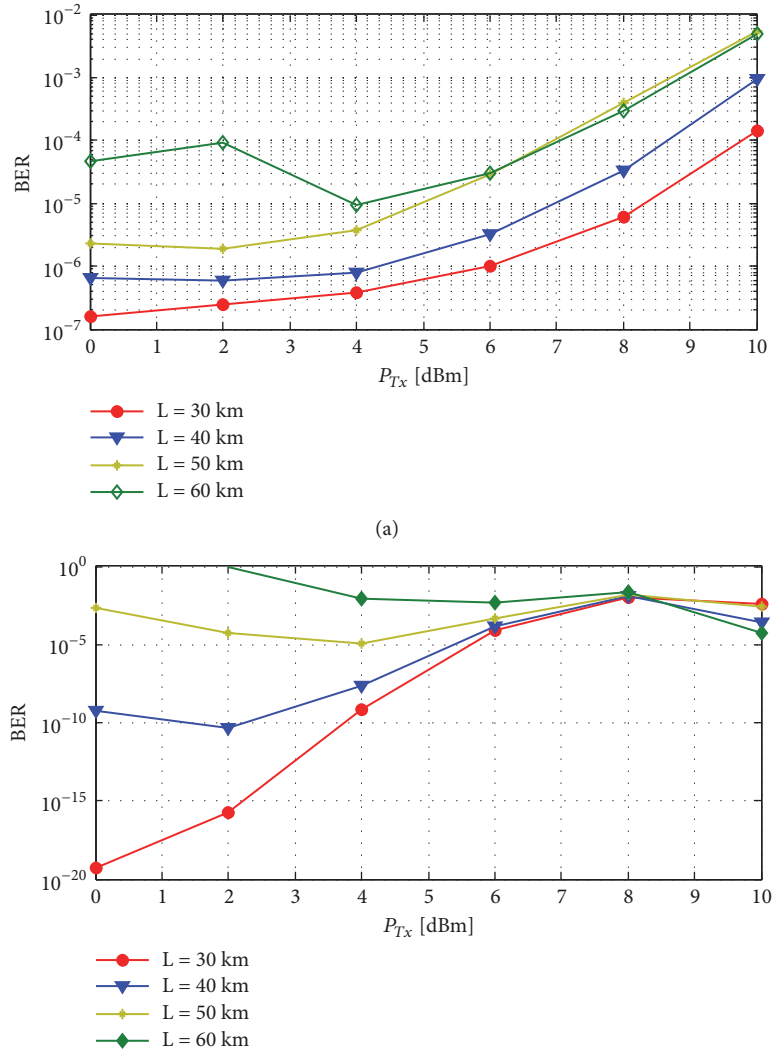

FIGURE 16: BER curves versus optical launch power for different fiber length values ($\Delta\alpha_{PDL}$ = 0.03 dB, $\Delta\vartheta = 5^{\circ}$, and f_{BR} = 10 Gbit/s) at (a) $\lambda \cong 1310$ nm; (b) $\lambda \cong 1550$ nm.

will be successful ($N_{burst\_received}$) and a certain number will be failed (N_{burst_lost}). The average values of these two numbers ($\overline{N_{burst\_received}}$ and $\overline{N_{burst\_lost}}$) are calculated to evaluate the burst loss probability p_{burst_loss} and the average throughput T of each link, defined as follows:

$$p_{burst\_loss} = \frac{\overline{N_{burst\_lost}}}{\overline{N_{burst\_lost}} + \overline{N_{burst\_received}}} \tag{12}$$

$$T = f_{BR} \bullet \left(1 - p_{burst\_loss}\right) \tag{13}$$

where $f_{BR} = 10\ Gbit/s$.

A simplified flow chart of the instructions executed in each iteration is represented in Figure 17. The code is structured in three main blocks: the description of the network, the generation of traffic bursts, and their routing among the nodes of the network. As it is stated in the third paragraph, each ROADM is a network node.

First of all, some global parameters are defined: the number of ROADM nodes (N); the number of ONUs (M) in each DWDM PON, coincident with the number of channels in each DWDM link; the traffic load, i.e., the percentage of active ONUs (rate); the percentage of VPNs ($\%_{VPN}$), i.e., the part of active ONUs asking to transmit towards other ONUs (the remaining part of active ONUs asks to transmit towards the OLT). Nodes and links are described through arrays whose atoms are two variable types defined as structures. The ith node is described by the variable $Node_i$ which has two fields: $Node_i.ONU_k$, i.e., the array of ONUs belonging to the WDM PON related to the node; $Node_i.prox_k$, i.e., the array of neighbor nodes. $Node_1$ is assumed to be the OLT. $Node_i.ONU_k$ is the k-th ONU belonging to the ith node. $Node_i.prox_k$ is the k-th neighbor node (the order of neighbors is not significant) belonging to the neighbor array of the ith node. The link between the ith node and the j-th node is described through the variable $NETWORK_{i,j}$ which

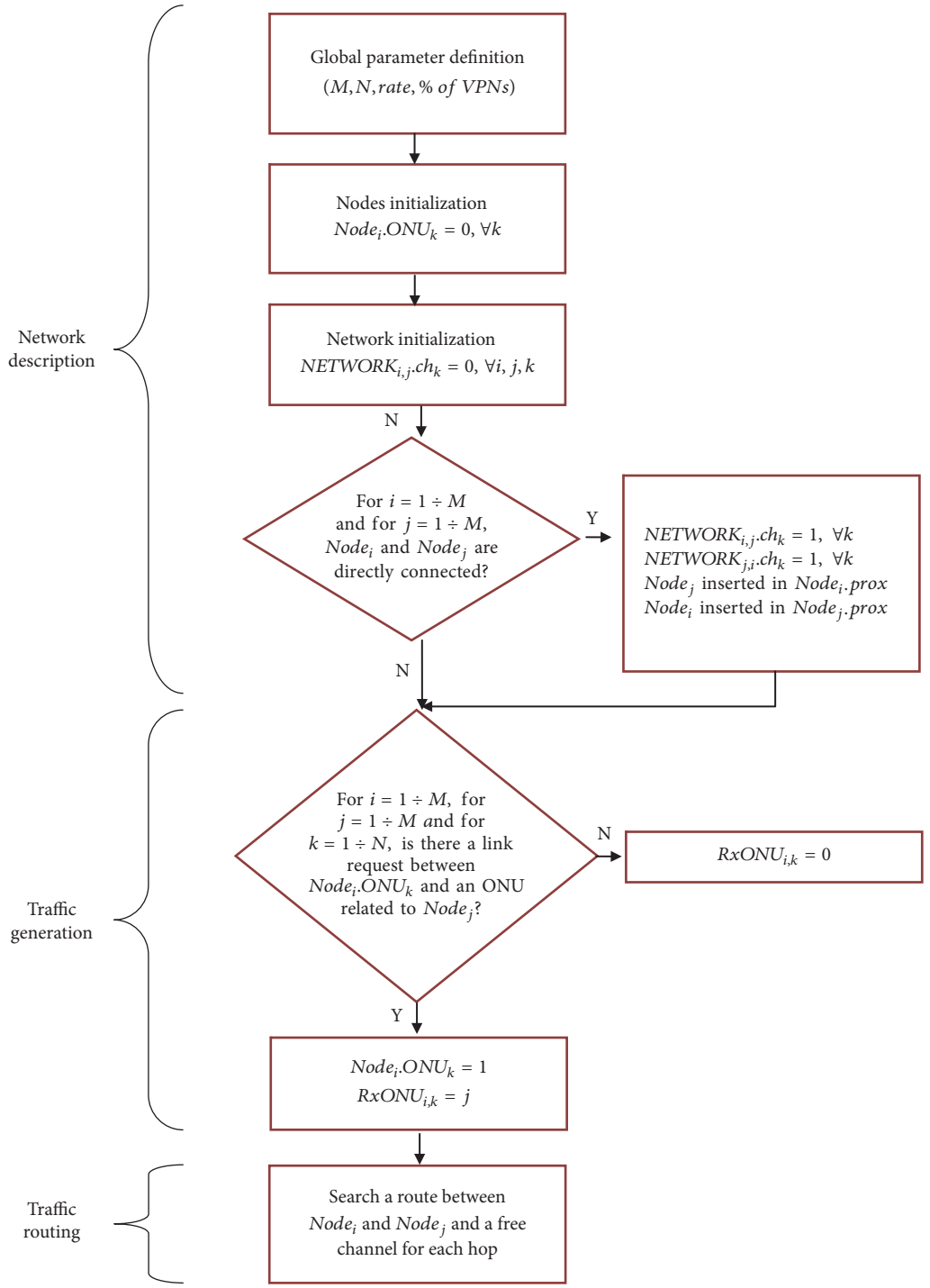

Figure 17: Simplified flow chart of each iteration of the Monte Carlo analysis to simulate network traffic.

has one field: $NETWORK_{i,j}.ch_k$, i.e., the array of channels constituting the link. The following assumptions have been adopted for ONUs and channels:

$$ONU_k = \begin{cases} 0 & ONU\ idle \\ 1 & ONU\ active, \end{cases} \quad k = 1, \ldots, M \tag{14}$$

$$ch_k = \begin{cases} 1 & channel\ available \\ 0 & channel\ busy\ or\ not\ existent, \end{cases} \quad k = 1, \ldots, M \tag{15}$$

Traffic generation is implemented by setting a percentage of ONUs ($\lfloor rate \bullet M \rceil$) in the active status: the active ONUs are determined by generating a pseudo-random sequence. For

a part of them ($\lfloor \%_{VPN} \bullet rate \bullet M \rceil$), the receiver node is determined as a pseudo-random number between 2 and N. For the remaining part of them the receiver node is set to 1, i.e., the OLT. In both cases the receiver ONUs can be chosen randomly, in this case between 1 and M. A $N \times M$ matrix of receiver nodes has been defined as follows:

$$RxONU_{i,k} = \begin{cases} 0 & Node_i.ONU_k = 0 \\ j & \text{link request between } Node_i.ONU_k \\ & \text{and an ONU belonging to } Node_j \end{cases} \quad (16)$$

Traffic routing is implemented through a recursive function whose input parameters are the transmitting node (i.e., the node associated with the transmitting ONU), the receiving node, and the number of the current hop. The function is called by the main application with the hop counter set to 1. In a few words, the routing function searches the receiving node ($Node_j$) among the neighbors of the transmitting node ($Node_i.prox$) and if there is any channel available to reach it ($k|NETWORK_{i,j}.ch_k = 1$). If the search has not a positive conclusion, the function invokes itself with the transmitting node set to each of its neighbors and the current hop incremented. The function can be invoked until the hop counter is less than N. The path is memorized through various function calls and, if the receiving node has been found, the function returns the route, i.e., the nodes and the channels involved. In this case, the main application allocates the corresponding network resources (by setting channels) and $N_{burst\_received}$ is incremented. Otherwise, N_{burst_lost} is incremented.

In order to ensure reproducibility of the Monte Carlo simulations, several details are presented hereafter: given a traffic load value, the number of experiments (iterations) performed is $N_{iterations} = 100$; therefore each value of the output variables (p_{burst_loss} and T) is calculated as the average of $N_{iterations} = 100$ values; a uniform distribution can be assumed for the pseudo-random sequences.

In order to evaluate traffic congestion according to various possible configurations of the proposed architecture, two kinds of simulations have been performed: p_{burst_loss} and T have been calculated by sweeping rate from 10% to 100% considering different values of $\%_{VPN}$ and different values of M.

In Figure 18 the results of the first typology of simulations is represented. If a given value of traffic load is considered, burst loss probability is higher if $\%_{VPN}$ is lower. These results can be explained in the following way: if the percentage of VPNs is lower, a higher part of the active ONU is transmitting towards the OLT; in this case, it is highly probable that the firstly saturated links are the ones connecting the OLT with the 3-way ROADMS. Since these links represent a bottleneck for the whole network, traffic congestion increases and performance decreases.

In Figure 19 the results of the second typology of simulations are given. If a given value of traffic load is considered, burst loss probability is lower if M is higher. These results can be explained in the following way: the higher M is, the higher the number of ONUs and the corresponding number of available channels are. In other words, a higher granularity of the information can be routed more efficiently with a reduced traffic congestion probability and an increased throughput.

7. Conclusions

An innovative metro-access architecture has been described. The topology and the physical working principles have been illustrated in detail. Some hints for the specific implementation of the optical subsystems in the network nodes have been given.

The proposed architecture presents the following key features. It merges metro and access segments, it performs optical switching based on OBS, it allows reconfigurability at the physical layer based on the separation between control plane and data plane thanks to PolDM, and it enables traffic management and optimization thanks to a centralized controller.

The feasibility of an optical metro-access network has been investigated, the most impactful impairments have been considered, and the main performance has been assessed.

Taking into account both PMD and PDL, over a fiber length of $L = 60$ km and considering a bit-rate $f_{BR} = 10$ Gbit/s, performance can be considered acceptable for a misalignment $\Delta\vartheta < 7^\circ$ between the SOP of the received signal and the SOP of the PBS used at the receiver, if the PDL coefficient is kept at $\Delta\alpha_{PDL} = 0.03$ dB. If a misalignment $\Delta\vartheta = 5^\circ$ is considered, under the same conditions, performance can be considered acceptable for a PDL coefficient $\Delta\alpha_{PDL} < 0.6dB$. If $\Delta\vartheta = 5^\circ$ and $\Delta\alpha_{PDL} = 0.03$ dB, over a fiber length of $L = 40$ km, performance is good (BER $< 10^{-4}$) until the launch power is kept under 6 dBm. The analysis of network congestion has demonstrated that burst loss probability can be kept under $p_{burst\_loss} = 10\%$ and throughput over $T = 9$ Gbit/s even if traffic load reaches 60% (considering half of the connection due to VPN traffic).

Of course, some aspects of the present proposal deserve further development. Colorless ONUs have to be compliant with the proposed architecture and should implement also algorithms for burst assembly. Furthermore the BHPG has to be designed according to the hints given in Section 4. The application layer on the controller has to be designed, i.e., the algorithms for network traffic orchestration exploiting the reconfigurability available at the physical layer. Since the algorithmic implementation of the controller has not been fully defined in this work, the protocol to be adopted for node configuration would be object of future works. Its compatibility with existing SDN standards and proposals should be investigated.

Data Availability

The data used to support the findings of this study are available from the corresponding author upon request.

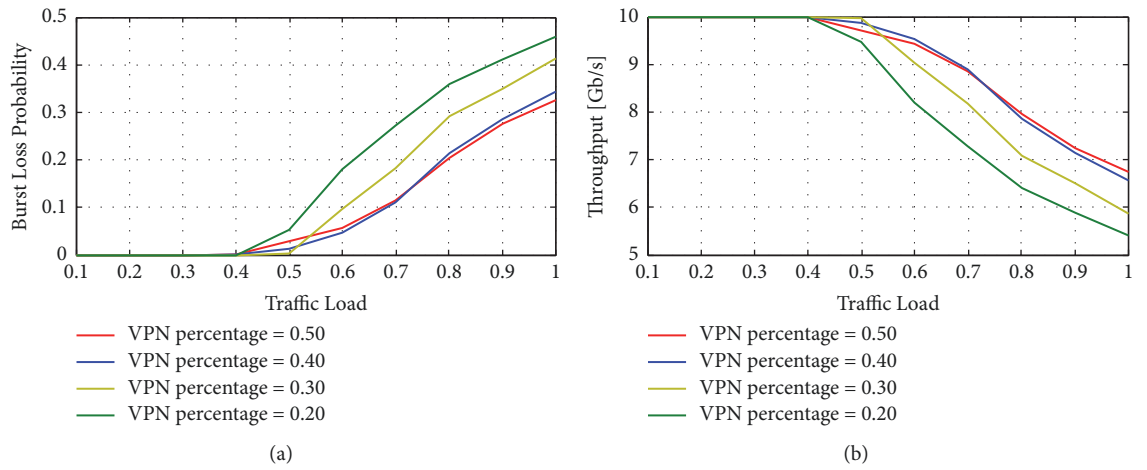

Figure 18: Network congestion for different values of $\%_{VPN}$: (a) burst loss probability versus traffic load; (b) throughput versus traffic load (N = 8, M = 100).

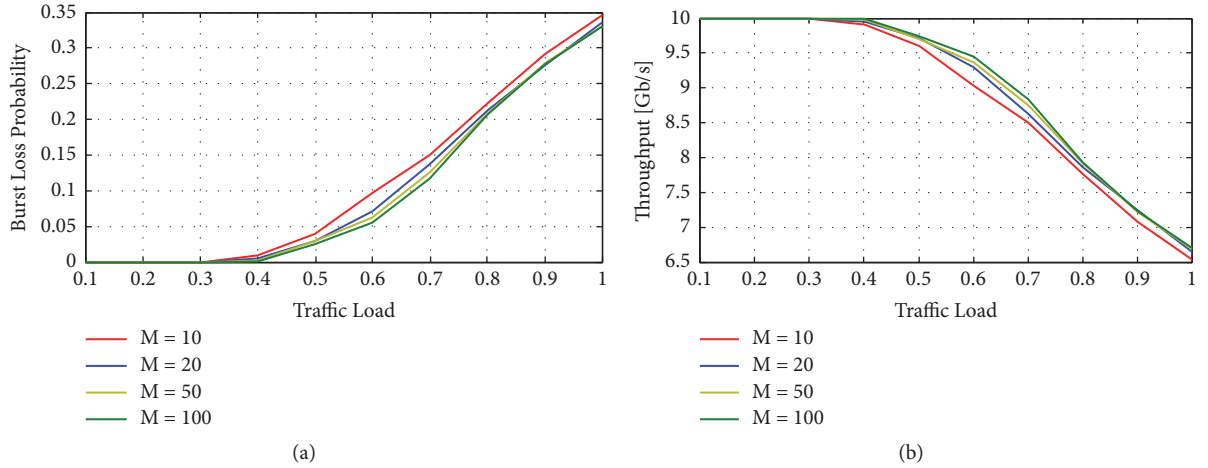

Figure 19: Network congestion for different values of M: (a) burst loss probability versus traffic load [12]; (b) throughput versus traffic load (N = 8, $\%_{VPN}$ = 0.5).

Conflicts of Interest

The authors declare that they have no conflicts of interest.

References

[1] N. Sambo, G. Meloni, F. Paolucci et al., "Programmable transponder, code and differentiated filter configuration in elastic optical networks," *Journal of Lightwave Technology*, vol. 32, no. 11, pp. 2079–2086, 2014.

[2] T. Muciaccia and V. M. N. Passaro, "Future scenarios for software-defined metro and access networks and software-defined photonics," *Photonics*, vol. 4, no. 1, pp. 1–27, 2017.

[3] P. Parol and M. Pawlowski, "Towards networks of the future: Sdn paradigm introduction to pon networking for business applications," in *Proceedings of the Conference on Computer Science and Information Systems*, pp. 829–836, Krakow, Poland, 2013.

[4] A. Amokrane, J. Hwang, J. Xiao, and N. Anerousis, "Software defined enterprise passive optical network," in *Proceedings of the 2014 10th International Conference on Network and Service Management (CNSM)*, pp. 406–411, Rio de Janeiro, Brazil, November 2014.

[5] Y. Lin, J. Zhang, J. Han et al., "Experimental demonstration of remote unified control for OpenFlow-based software-defined optical access networks," *Photonic Network Communications*, vol. 31, pp. 568–575, 2015.

[6] F. Vacondio, J. Antona, G. de Valicourt et al., "Flexible TDMA access optical networks enabled by burst-mode software defined coherent transponders," in *Proceedings of the 39th European Conference and Exhibition on Optical Communication (ECOC 2013)*, pp. 393–395, London, UK, September 2013.

[7] N. Cvijetic, A. Tanaka, P. N. Ji, K. Sethuraman, S. Murakami, and T. Wang, "SDN and openflow for dynamic flex-grid optical access and aggregation networks," *Journal of Lightwave Technology*, vol. 32, no. 4, pp. 864–870, 2014.

[8] S. Yin, T. S. Shen, and L. G. Kazovsky, "UltraFlow: Elastic, flexible and dual-mode long-reach optical access network," in *Proceedings of the 2015 International Conference on Computing,*

Networking and Communications (ICNC), pp. 837–841, Anaheim, CA, USA, Feburary 2015.

[9] E. Yetginer and E. Karasan, "Dynamic wavelength allocation in IP/WDM metro access networks," *IEEE Journal on Selected Areas in Communications*, vol. 26, no. 3, pp. 13–27, 2008.

[10] T. Muciaccia and S. Pileri, "Riconfigurabilità nelle reti di accesso e metro-access," *Notiziario Tecnico - Telecom Italia*, vol. 1, pp. 108–121, 2016.

[11] T. Muciaccia and V. Passaro, "A novel SDN-like DWDM all-optical metro-access network architecture," in *Proceedings of the 18th Italian National Conference on Photonic Technologies (Fotonica 2016)*, pp. 1–4, Rome, Italy, 2016.

[12] T. Muciaccia and V. Passaro, "Performance characterization of a novel DWDM all-optical SDN-like metro-access network," in *Proceedings of the International Conference on Software, Telecommunications and Computer Networks*, Split, Croatia, 2016.

[13] T. Muciaccia, F. Gargano, and V. M. N. Passaro, "Passive optical access networks: State of the art and future evolution," *Photonics*, vol. 1, no. 4, pp. 323–346, 2014.

[14] K. Grobe and J.-P. Elbers, "PON in adolescence: from TDMA to WDM-PON," *IEEE Communications Magazine*, vol. 46, no. 1, pp. 26–34, 2008.

[15] F. R. Barbosa, E. Moschim, and I. B. Martins, "Future-proof photonic switched optical networks for metropolitan access," in *Proceedings of the 2012 Symposium on Photonics and Optoelectronics (SOPO 2012)*, pp. 1–6, Shanghai, China, May 2012.

[16] I. B. Martins, F. R. Barbosa, L. H. Bonani, and E. Moschim, "Impact of link failure in the performance of optical OPS/OBS limited-area networks with node ingress buffering," in *Proceedings of the 11th International Conference on Telecommunications, ConTEL 2011*, pp. 325–332, Graz, Austria, June 2011.

[17] A. N. Patel, P. N. Ji, and T. Wang, "QoS-aware optical burst switching in openflow based software-defined optical networks," in *Proceedings of the International Conference on Optical Network Design and Modeling*, pp. 275–280, Brest, France, 2013.

[18] R. Nejabati, G. Zervas, G. Dimitriades, and D. Simeonidou, "Programmable optical burst switched network: a novel infrastructure for grid services," in *Proceedings of the IEEE International Symposium on Cluster Computing and the Grid*, pp. 993–999, Cardiff, Wales, UK, May 2005.

[19] S. J. B. Yoo, "Optical packet and burst switching technologies for the future photonic internet," *Journal of Lightwave Technology*, vol. 24, no. 12, pp. 4468–4492, 2006.

[20] S. Gringeri, N. Bitar, and T. Xia, "Extending software defined network principles to include optical transport," *IEEE Communications Magazine*, vol. 51, no. 3, pp. 32–40, 2013.

[21] E. J. Klein, D. H. Geuzebroek, H. Kelderman, G. Sengo, N. Baker, and A. Driessen, "Reconfigurable optical add-drop multiplexer using microring resonators," *IEEE Photonics Technology Letters*, vol. 17, no. 11, pp. 2358–2360, 2005.

[22] Q. Xu, V. R. Almeida, and M. Lipson, "Micrometer-scale all-optical wavelength converter on silicon," *Optics Expresss*, vol. 30, no. 20, pp. 2733–2735, 2005.

[23] I. S. Amiri, S. E. Alavi, and S. M. Idrus, *Soliton Coding for Secured Optical Communication Link*, Springer, 2015.

[24] T. Muciaccia, F. Gargano, and V. Passaro, "A reconfigurable optical metro-access network and an innovative ROADM for efficient dynamical bandwidth allocation," in *Proceedings of the 2015 Fotonica AEIT Italian Conference on Photonics Technologies*, pp. 1–4, Turin, Italy, May 2015.

[25] D. Nesset, T. Kelly, and D. Marcenac, "All-optical wavelength conversion using SOA nonlinearities," *IEEE Communications Magazine*, vol. 36, no. 12, pp. 56–61, 1998.

[26] T. Durhuus, B. Mikkelsen, C. Joergensen, S. L. Danielsen, and K. E. Stubkjaer, "All-optical wavelength conversion by semiconductor optical amplifiers," *Journal of Lightwave Technology*, vol. 14, no. 6, pp. 942–954, 1996.

[27] Y. Liu, E. Tangdiongga, Z. Li et al., "Error-free 320-Gb/s all-optical wavelength conversion using a single semiconductor optical amplifier," *Journal of Lightwave Technology*, vol. 25, no. 1, pp. 103–108, 2007.

[28] Y. Liu, J. Herrera, O. Raz et al., "160 Gbit/s all-optical SOA-based wavelength conversion and error-free transmission through two 50 km fibre links," *IEEE Electronics Letters*, vol. 43, no. 25, pp. 1447–1449, 2007.

[29] M. Matsuura, O. Raz, F. Gomez-Agis, N. Calabretta, and H. J. S. Dorren, "Ultrahigh-speed and widely tunable wavelength conversion based on cross-gain modulation in a quantum-dot semiconductor optical amplifier," *Optics Express*, vol. 19, no. 26, pp. B551–B559, 2011.

[30] V. Eramo, A. Germoni, A. Cianfrani, M. Listanti, and C. Raffaelli, "Evaluation of power consumption in low spatial complexity optical switching fabrics," *IEEE Journal of Selected Topics in Quantum Electronics*, vol. 17, no. 2, pp. 396–405, 2011.

[31] C. Stamatiadis, K. Vyrsokinos, L. Stampoulidis et al., "All-optical wavelength conversion at 160Gb/s using an SOA and a 3rd order SOI nanowire periodic filter," in *Proceedings of the 23rd Annual Meeting of the IEEE Photonics Society, PHOTINICS 2010*, pp. 268-269, Denver, CO, USA, November 2010.

[32] P. P. Iannone and K. C. Reichmann, "Hybrid SOA-raman amplifiers for fiber-to-the-home and metro networks," in *Proceedings of the 2008 Conference on Optical Fiber Communication - OFC 2008 Collocated National Fiber Optic Engineers*, pp. 1–8, San Diego, CA, USA, Feburary 2008.

[33] T. Muciaccia, F. Gargano, and V. M. N. Passaro, "A TWDM-PON with advanced modulation techniques and a multi-pump raman amplifier for cost-effective migration to future UDWDM-PONs," *Journal of Lightwave Technology*, vol. 33, no. 14, pp. 2986–2996, 2015.

[34] S. Lewis, S. Chernikov, and J. Taylor, "1.4 W saturated output power from a fibre Raman amplifier," in *Proceedings of the OFC/IOOC'99. Optical Fiber Communication Conference and the International Conference on Integrated Optics and Optical Fiber Communications*, pp. 114–116, San Diego, CA, USA, 1999.

[35] C. Codemard, P. Dupriez, Y. Jeong, J. Sahu, M. Ibsen, and J. Nilsson, "High power cladding-pumped Raman fiber laser with true single-mode output at 1660 nm," in *Proceedings of the OFCNFOEC 2006. 2006 Optical Fiber Communication Conference and the National Fiber Optic Engineers Conference*, p. 3, Anaheim, CA, USA, March 2006.

[36] C. Codemard, J. Sahu, and J. Nilsson, "High-brightness, pulsed, cladding-pumped Raman fiber source at 1660 nm," in *Proceedings of the CLEO 2007*, pp. 1-2, Baltimore, MD, USA, May 2007.

[37] J. A. Nagel, V. Temyanko, J. Dobler et al., "High-power narrow-linewidth continuous-wave Raman amplifier at 1.27 μm," *IEEE Photonics Technology Letters*, vol. 23, no. 9, pp. 585–587, 2011.

[38] J. W. Fleischer, G. Bartal, O. Cohen et al., "Spatial photonics in nonlinear waveguide arrays," *Optics Express*, vol. 13, no. 6, pp. 1780–1796, 2005.

[39] P. W. Juodawlkis and J. J. Plant, "Gain-power trade-off in low-confinement semiconductor optical amplifiers," in *Proceedings*

of the 7th International Conference on Numerical Simulation of Optoelectronic Devices. NUSOD'07, pp. 97-98, Newark, DE, USA, September 2007.

[40] K. Morito, S. Tanaka, S. Tomabechi, and A. Kuramata, "A broad-band MQW semiconductor optical amplifier with high saturation output power and low noise figure," *IEEE Photonics Technology Letters*, vol. 17, no. 5, pp. 974–976, 2005.

[41] J. Klamkin, J. Plant, M. Sheehan, W. Loh, S. Madison, and P. Juodawlkis, "High-output saturation power variable confinement slab-coupled optical waveguide amplifier," in *Proceedings of the National Fiber Optic Engineers Conference*, Los Angeles, Ca, USA, March 2011.

[42] T. W. Berg and J. Mørk, "Quantum dot amplifiers with high output power and low noise," *Applied Physics Letters*, vol. 82, no. 18, pp. 3083–3085, 2003.

[43] Z. Bakonyi, H. Su, G. Onishchukov et al., "High-gain quantum-dot semiconductor optical amplifier for 1300 nm," *IEEE Journal of Quantum Electronics*, vol. 39, no. 11, pp. 1409–1414, 2003.

[44] J. Baliga, R. Ayre, W. V. Sorin, K. Hinton, and R. S. Tucker, "Energy consumption in access networks," in *Proceedings of the 2008 Conference on Optical Fiber Communication - OFC 2008 Collocated National Fiber Optic Engineers*, pp. 1–3, San Diego, CA, USA, Feburary 2008.

[45] J. Baliga, R. Ayre, K. Hinton, W. V. Sorin, and R. S. Tucker, "Energy consumption in optical IP networks," *Journal of Lightwave Technology*, vol. 27, no. 13, pp. 2391–2403, 2009.

[46] Optokon, "OLT LTP-8X central office node terminal (GPON)," Data sheet. http://www.optokon.com/olt-ltp-8x-central-office-node-terminal-gpon-0.

[47] E. Murphy, C. Michie, H. White, W. Johnstone, and I. Andonovic, "Power savings in a wavelength-division-multiplexed passive optical network for aircraft," *Optical Engineering*, vol. 53, no. 12, p. 126109, 2014.

[48] Thorlabs, "DWDM Laser Sources for TXP5000 – LS5000 Series," Data sheet, https://www.thorlabs.de/catalogpages/V21/1275.PDF.

[49] B. R. Koch, A. W. Fang, R. Jones et al., "Silicon evanescent optical frequency comb generator," in *Proceedings of the 2008 5th IEEE International Conference on Group IV Photonics (GFP)*, pp. 64–66, Sorrento, Italy, September 2008.

[50] R. Slavík, J. Kakande, P. Petropoulos, and D. J. Richardson, "Processing of optical combs with fiber optic parametric amplifiers," *Optics Express*, vol. 20, no. 9, p. 63590, 2012.

[51] V. Corral, R. Guzmán, C. Gordón, X. J. M. Leijtens, and G. Carpintero, "Optical frequency comb generator based on a monolithically integrated passive mode-locked ring laser with a Mach-Zehnder interferometer," *Optics Expresss*, vol. 41, no. 9, pp. 1937–1940, 2016.

[52] P. Del'Haye, A. Schliesser, O. Arcizet, T. Wilken, R. Holzwarth, and T. J. Kippenberg, "Optical frequency comb generation from a monolithic microresonator," *Nature*, vol. 450, no. 7173, pp. 1214–1217, 2007.

[53] R. Wu, V. R. Supradeepa, C. M. Long, D. E. Leaird, and A. M. Weiner, "Generation of very flat optical frequency combs from continuous-wave lasers using cascaded intensity and phase modulators driven by tailored radio frequency waveforms," *Optics Expresss*, vol. 35, no. 19, pp. 3234–3236, 2010.

[54] R. Lin, M. Tang, R. Wang et al., "An ultra-dense optical comb based DWDM-OFDM-PON system," in *Proceedings of the Progress in Electromagnetics Research Symposium*, Guangzhou, China, August 2014.

[55] A. R. Chraplyvy, A. H. Gnauck, R. W. Tkach et al., "1-Tb/s transmission experiment," *IEEE Photonics Technology Letters*, vol. 8, no. 9, pp. 1264–1266, 1996.

[56] ITU-T G.984.3, "Gigabit-capable passive optical networks (G-PON): transmission convergence layer specification," 2008.